Available online at website: https://journal.bcrec.id/index.php/bcrec

Bulletin of Chemical Reaction Engineering & Catalysis, 19 (3) 2024, 418-428

Research Article

Optimization of TiO_2-based UV-LED Photocatalytic System for Mixed Dyes and Pharmaceutical Contaminants

Zexiang Chen[1], Xue Kang[2,4], Chen Wang[3,4], Yonguo Li[1,*]

[1]Key Laboratory of Nuclear Air Purification Technology, China Institute for Radiation Protection, Taiyuan, Shanxi, 030006, China.
[2]School of Environment and Safety Engineering, North University of China, Taiyuan 030051, China.
[3]School of Chemistry and Chemical Engineering, North University of China, Taiyuan 030051, China.
[4]Dezhou Industrial Technology Research Institute of North University of China, Dezhou 253000, China.

Received: 10th July 2024; Revised: 3rd August 2024; Accepted: 4th August 2024
Available online: 25th August 2024; Published regularly: October 2024

Abstract

To optimize the working efficiency of the novel UV-LED system based on TiO_2 photocatalyst, the influence mechanism of LED lamp arrangement, light source wavelength and working voltage on photocatalytic efficiency was investigated. Acid red 26 (AR 26), acetaminophen (ACT) and diclofenac (DCF) were used as contaminant targets of the photocatalytic system. LED lamp arrangement had almost no effect on the degradation of AR26. However, the degradation efficiency of ACT and DCF was improved under a higher light uniformity. The ACT concentration and DCF concentration at 360 min decreased by 14% and 15%, respectively, with increasing light distribution from 45% to 66.5%. The main reason for this discrepancy in effect was whether the rate-determining step of the degradation mechanism was affected by the light uniformity. The short wavelength and high working voltage of LEDs were conducive to the photocatalytic degradation of contaminants to a different degree. When the wavelength was reduced from 405nm to 365nm, the conversion of AR26, ACT, and DCF increased by 77%, 227%, and 106%, respectively. The conversion rates of AR26, ACT, and DCF increased by 28%, 54%, and 32%, respectively, with voltage increasing from 3 V to 4 V. The data of this work will provide support for optimizing the working efficiency of UV-LED systems based on TiO_2 photocatalysts.

Keywords: TiO_2 photocatalyst; UV-LED; Lamp arrangement; wavelength; working voltage

How to Cite: Z. Chen, X. Kang, C. Wang, Y. Li (2024). Optimization of TiO_2-based UV-LED Photocatalytic System for Mixed Dyes and Pharmaceutical Contaminants. *Bulletin of Chemical Reaction Engineering & Catalysis*, 19 (3), 418-428 (doi: 10.9767/bcrec.20180)

Permalink/DOI: https://doi.org/10.9767/bcrec.20180

1. Introduction

Wastewater treatment involves all aspects of human life and industrial production. With the rapid development of the printing and dyeing industry, printing and dyeing wastewater is refractory due to its high concentration of pollutants and complex composition, seriously affecting the water environment [1-3]. Azo dyes, which account for 70% of synthetic dyes in wastewater, are carcinogenic and inhibit the growth of aquatic life [4,5]. The azo structure (−N=N−) is one of the key factors that makes printing and dyeing wastewater difficult to degrade. Besides, pharmaceuticals and personal care products (PPCPs) often exist in water[6]. It has drawn much attention due to the complicated organic compounds involved in PPCPs.

Physical [7,8], biological [9,10], and electrochemical [11,12] methods were proposed to degrade azo dyes and organic compounds. However, biological methods make it difficult to decolorize printing and dyeing wastewater with poor biodegradability. Pharmaceuticals are generally recalcitrant to biochemical process. Adsorption methods require specificity for the adsorbent and the adsorbent lifetime is often short. Electrochemical methods consume too

* Corresponding Author.
Email: lyg0624@163.com (Y. Li)

much energy, and traditional treatment processes produce a large amount of sludge and require secondary treatment. The photocatalytic oxidation method has attracted widespread attention due to its simple operation, short treatment cycle, and no harmful by-products. This technology employs active free radicals (hydroxyl and oxygen free radicals) to effectively decompose contaminants [13-15]. For the removal of organic compounds from wastewater, TiO_2-based photocatalytic technologies were studied by researchers due to the stable self-regeneration of free radicals via UV light exposure [16,17]. A high-power light-emitting diode (LED) offers the UV source the advantage of high efficiency, stable working power, short start-up time and long life span [18]. However, the temperature of the LED chips would increase dramatically if the heat dissipation was not well operated [19]. Many studies have reported on how to improve the cooling efficiency of LED-UV systems. Chen *et al*. found that an air-cooled radiator and a water-cooled microchannel radiator should be used for the low-power LED chipsets and the high-power LED chipsets, respectively [20]. Seo *et al*. proposed that the cooling performances could be improved by using the ferrofluid as the cooling medium, and the fin heat sink filled with the ferrofluid was also suggested [21]. In general, the liquid as the cooling medium was better than the gas. Our previous work proposed that dyeing wastewater itself was an excellent and low-cost cooling fluid [22]. A novel TiO_2-based photocatalytic system of UV-LED coupling with a wastewater cooler cycle was constructed. the TiO_2/UV-LED photocatalytic system has attracted increasing attention from the academic community due to its low cost and high energy efficiency, especially in the treatment of pharmaceutical contaminants [23].

Many factors can affect the efficiency of this novel system. All factors that affect the heat dissipation efficiency of LED lights, such as the composition and concentration of wastewater, wastewater flow rate, wastewater temperature, catalyst selection, pH, *etc*., indirectly lead to different efficiencies of wastewater decomposition. Our previous study found that a low temperature (20 °C) of wastewater improved the long-term operational stability of LED beads, a moderate dose of TiO_2 with strong acid condition (pH=2) further improved the photocatalytic activity. In addition, the effects of the arrangement of LED lights, the range of LED light wavelengths, and system working voltage on the efficiency of the TiO_2/UV-LED photocatalytic system are few reported. Previous research reports often only explored the degradation performance of a single pollutant, either azo dyes or one type of organic compound [24]. Few studies on sewage systems where multiple contaminants coexist were reported. Acid red 26 (AR 26) is a typical fuel dye. Acetaminophen (ACT) and diclofenac (DCF) were typical analgesic drugs and anti-inflammatory drugs in the pharmaceutical industry, respectively.

In this work, the TiO_2-based photocatalytic system of UV-LED is optimized. By studying the impact of the arrangement of LED lights, the LED light wavelengths, and the system working voltage on photocatalytic degradation of multiple contaminants, the optimal working conditions of

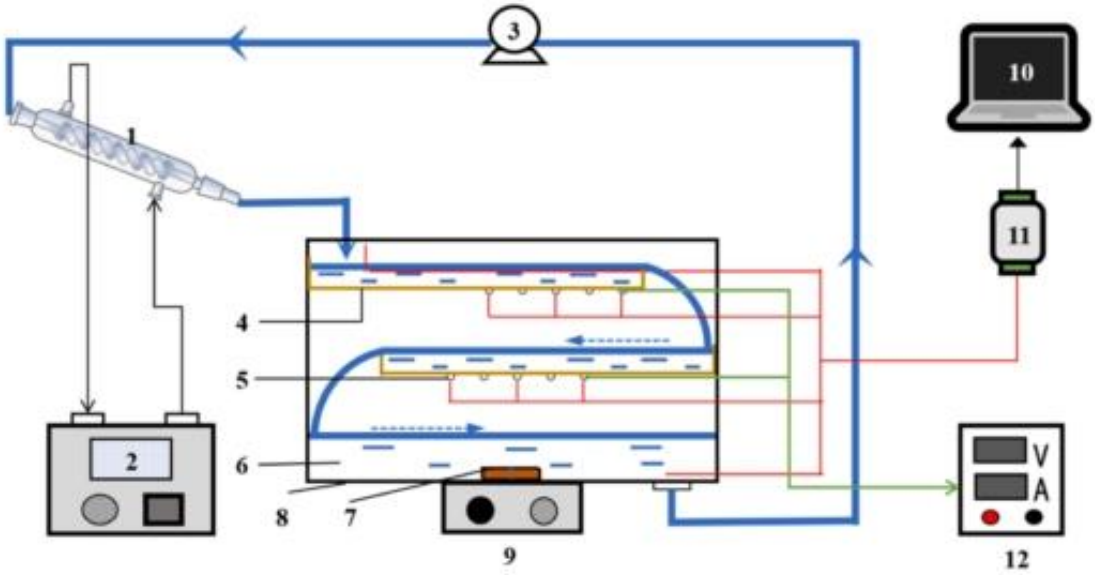

Figure 1. Scheme of the TiO_2-based UV-LED system. (1. Condenser, 2. Thermostatic water bath, 3. Water pump, 4. Copper plate, 5. UV-LED beads, 6. Wastewater, 7. Magnetron, 8. Water storage bath, 9. Magnetic stirrer, 10. Laptop, 11. Temperature sensor, 12. DC power.)

the system were revealed. The degradation of AR 26, ACT and DCF was investigated under different optimized conditions. This work would provide data support for further realizing the engineering application of UV-LED photocatalytic systems.

2. Materials and Methods

The experimental system (Figure 1) is the same as the previously reported [22,25]. The simulated wastewater flows through the heat exchange copper plate of the LED lamp and the sewage tank and circulates at a flow rate of 80 mL/min. AR 26 was bought from Ruji Technology Development Co., ltd China. ACT and DCF were supplied from Sigma-Aldrich, USA. 20 mg/L AR 26, 20 mg/L ACT, 20 mg/L DCF and 0.2 g/L TiO_2 are well dispersed in the 4L deionized water by violently stirred for 40 min. When operating, a constant current DC source (Dazheng, PS-305D 0~30 V/0~5 A) is used as the power supply for UV-LED. The concentration of AR 26 was measured by a UV-Vis spectrometer (Lambda 365, PerkinElmer, Inc., USA) at λ_{max} = 505.45 nm. A high-performance liquid chromatography with a UV detector (1260 infinity II, Agilent Technologies, USA) was used to measure ACT and DCF.

The numerical simulation is conducted with the commercial software TracePro. The light intensity distribution under different arrangements of UV-LEDs is calculated. In the model, as shown in Figure 2, the size of the LED substrate is set to 3.45 mm × 3.45 mm. The illumination angle of the LED lamp is set to 120°. The diameter of the upper and lower round table of the reflective bowl is 1.2 mm and 0.65 mm, respectively. The height of the reflector bowl is 0.9 mm. The chip is modeled as a cuboid with the size of 0.4 × 0.4 × 0.15 mm^3. The lens of LED is simplified as a thin cylinder with a diameter of 1.2 mm and a thickness of 0.01 mm. The 0.05 lm luminous flux and 385 nm wavelength are simulated, according to the product manual. 30% of emitted light energy is adopted as 0.345 W for a single lamp. Assume that light passes through the reflective bowl and lens without energy loss. An "ABg" bi-directional transmission distribution function (ABg BTDF) is used as the equation (1),

$$BTDF = \frac{A}{B + \left|\vec{\beta} - \vec{\beta}_0\right| g} \quad (1)$$

where, the β and β_0 vectors are from the Harvey-Shack BSDF model. The β vector is the projection of a unit vector in the scattering direction onto the tangent plane, and the β_0 vector is a projection of the unit vector in the specular direction onto the tangent plane. A, B, and g are fitting parameters where A determines the height of the curve, B determines the point where the curve transitions from flat to sloped and g determines the slope.

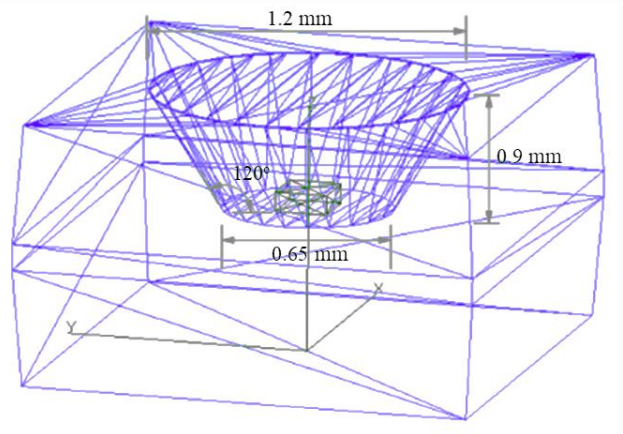

Figure 2. Model of LED lamp bead

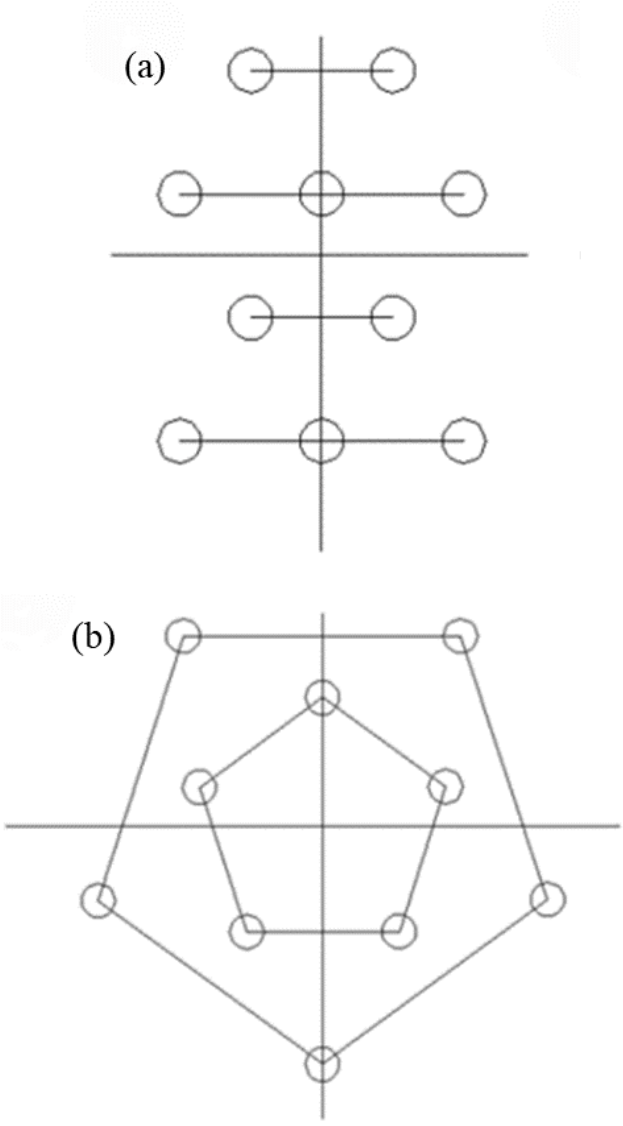

Figure 3. Two arrangement patterns of 10 LED lamp beads: (a) Pattern A and (b) Pattern B

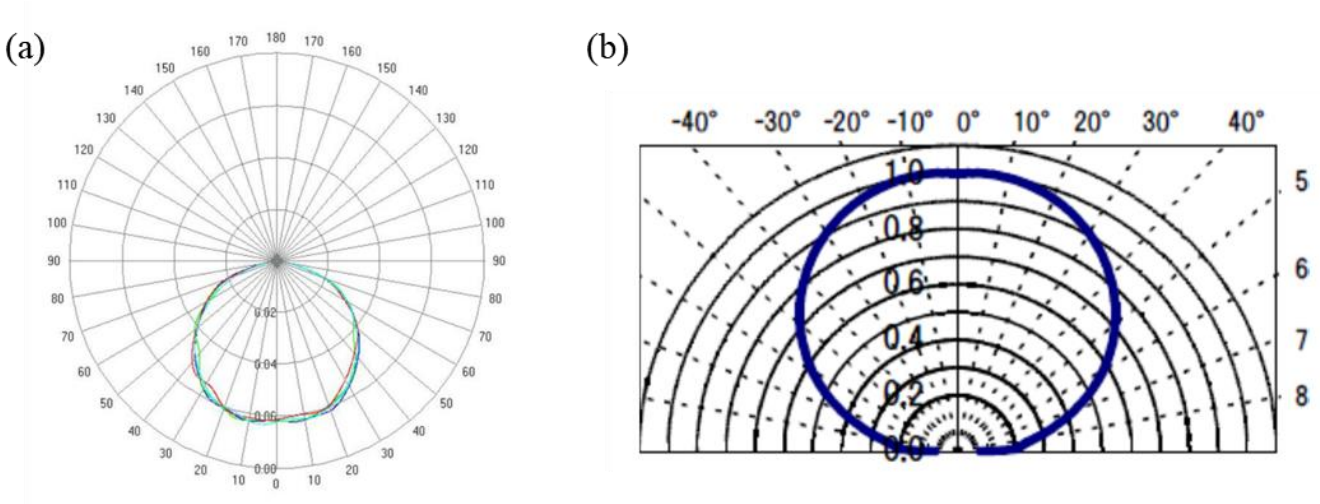

Figure 4. Simulated light distribution curve (a) and real light distribution curve from the manufacturer (b).

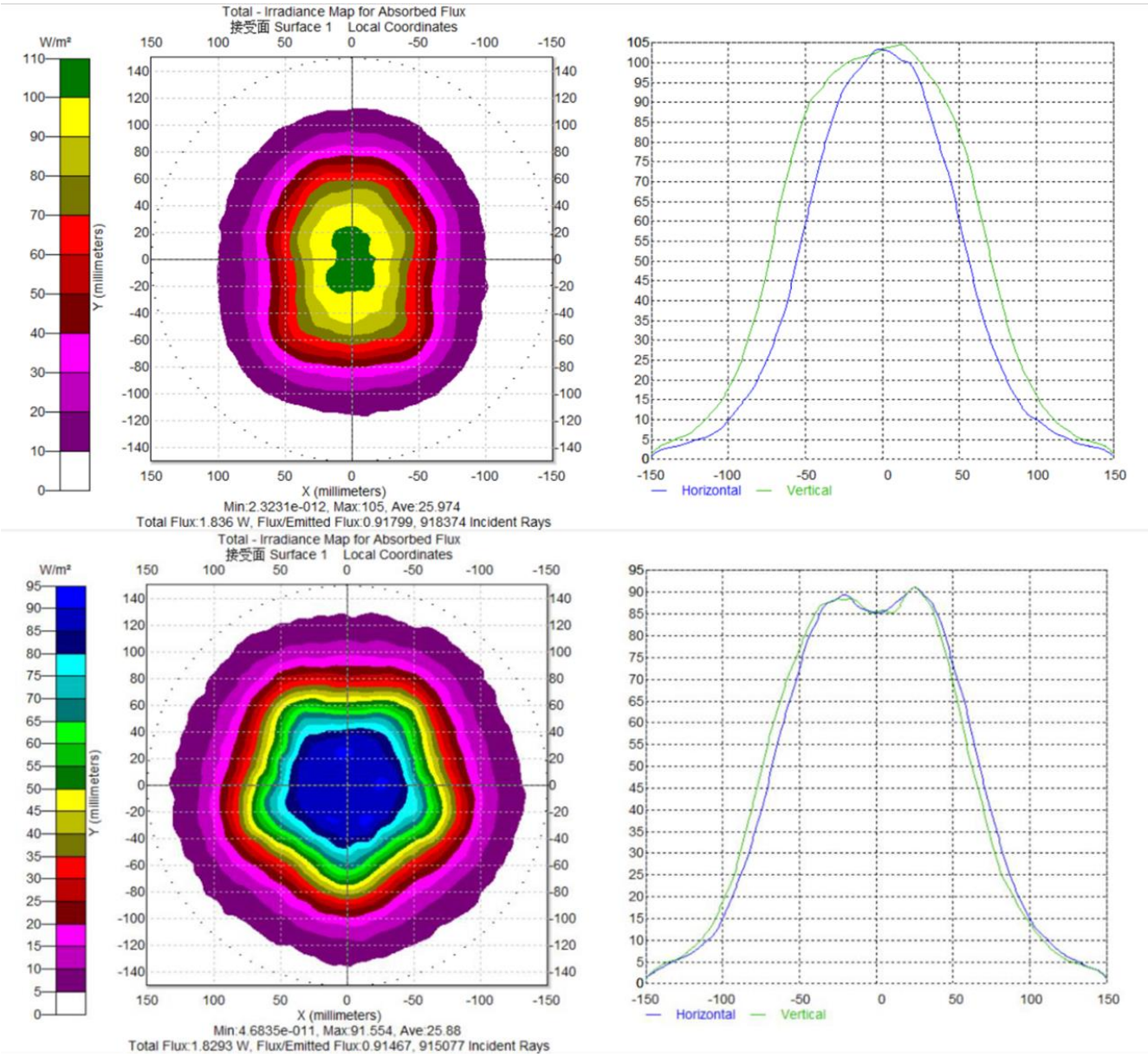

Figure 5. Spatial distribution of light intensity for two LED arrangement patterns.

Generally, *A*, *B*, and *g* are set to 0.35, 0.1, and 0 to model a perfect Lambertian surface. The Monte Carlo algorithm is employed to trace the ray emitted by the LED light source. Considering the calculation accuracy and cost, the total intercepts (traced rays) of ten LEDs for two patterns were set to 100,000 to ensure that the calculation is both efficient and accurate. 100 thousand rays are traced in the calculations for different arrangement patterns. Other reported simulations used similar parameter settings [26].

3. Results and Discussion

3.1 Effect of UV-LED Arrangement

To investigate the effect of LED arrangement on the degradation of wastewater and optimize the LED arrangement, two arrangement patterns of 10 LED lamp beads were examined, as shown in Figure 3. The light intensity was simulated using TracePro simulation software. The light distribution on the wastewater surface (length: 190mm) was calculated by a luminous map. Before calculation, the light distribution curve was validated. The simulated light distribution curve for a single LED lamp is shown in Figure 4(a). Compared to the light distribution curve (Figure 4(b)) offered by the manufacturer, the simulated light distribution curve has the same shape as the real light distribution curve, which shows the effectiveness of the simulation.

As shown in Figure 5, the light intensity emitted by UV-LED arrays for two arrangement patterns was simulated and analyzed. The luminous flux results on the receiving surface were presented in the form of an irradiation map. The luminous flux on the receiving surface was presented in the form of a ground view. The luminous flux distribution along the horizontal axis section (Y=0) and the vertical axis section (X=0) is also shown in Figure 5. The results showed that the light intensity of pattern A was more concentrated than that of pattern B. In contrast, the light intensity distribution range of pattern B is wider than that of pattern A. This set of comparison tests controlled the total incident flux and changed the spatial distribution of light.

All the ultraviolet light beams fell within the boundary range (dashed circle). The minimum, maximum, average irradiance and light uniformity can be obtained, as shown in Table 1. Based on the standard of ANSI/NAPMIT7.228-1997 [27], the irradiation uniformity can be calculated. The average light intensity of the two arrangements was close, which was reasonable due to the same total incident illumination. The light uniformity of pattern A (66.5%) was higher than that of pattern B (45.0%).

To determine the effect of LED arrangement on the degradation rate of AR 26, ACT and DCF, the concentrations of them were detected, as shown in Figure 6. The results showed that the degradation trend of AR 26 has not changed under the two arrangements. However, different LED arrangements had a significant impact on the degradation of ACT and DCF, which degraded

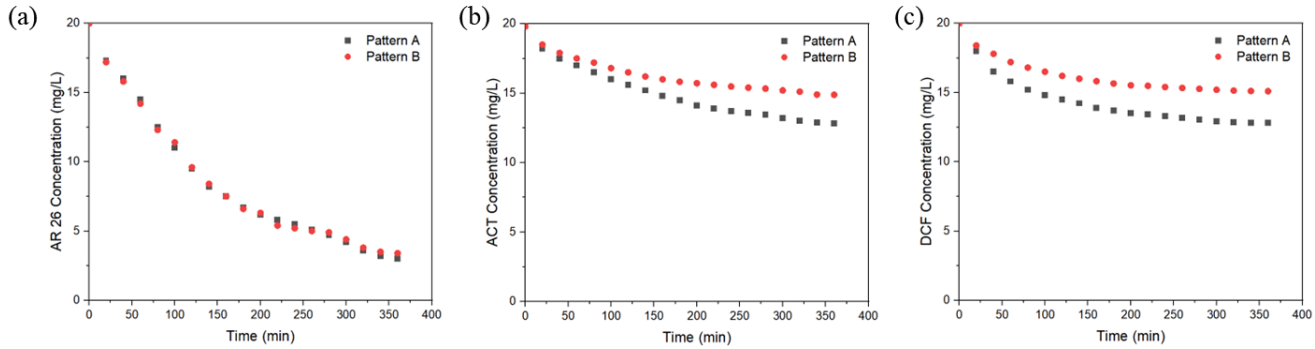

Figure 6. Evolution of concentrations of (a) AR 26, (b) ACT and (c) DCF under two different LED lamp arrangements.

Table 1. Light distribution properties of two different LED arrangements.

Arrangement	E_{min}[1] (W/m^2)	E_{max}[1] (W/m^2)	E_{ave}[2,*] (W/m^2)	Light uniformity (%)
Pattern A	2.3×10^{-12}	105.0	25.97	66.5
Pattern B	4.7×10^{-11}	91.6	25.88	45.0

1. E_{min}, E_{max} and E_{ave} represented the minimum, maximum and average irradiance over the statistical range.

2. $$E_{ave} = \frac{\int\int_{-0.15}^{0.15} Irradiance(x,y)\,dxdy}{\pi 0.15^2}$$

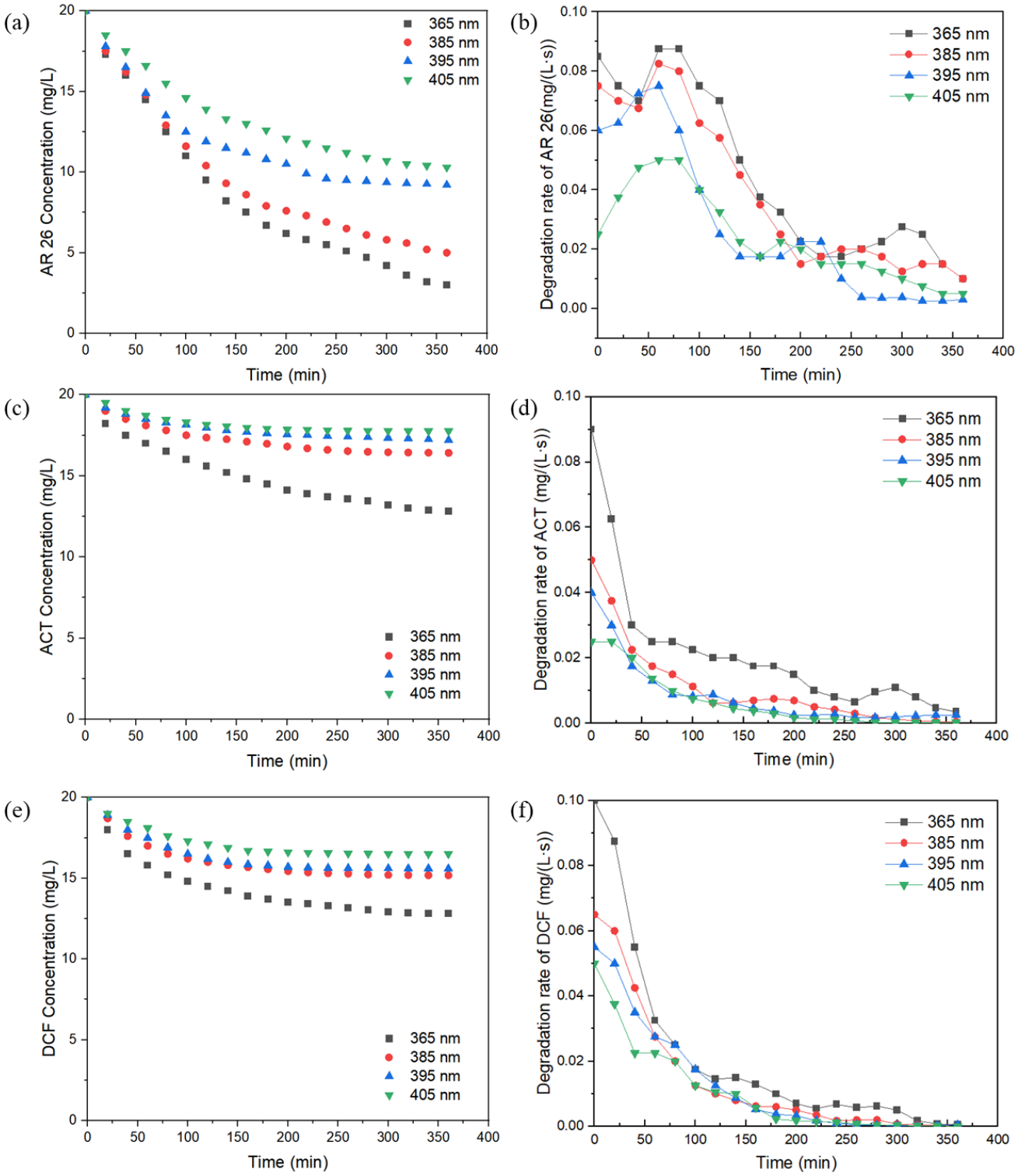

Figure 7. Evolution of the AR 26 concentration and the reaction rate with the different UV LED wavelengths.

Table 2. Specification of UV-LED photoreactor with different wavelengths and the conversion of AR 26 after 360 min reaction.

Wavelength (nm)	Output power (mW)	Voltage (V)	AR 26 conversion (%)	ACT conversion (%)	DCF conversion (%)
365	300	3.2~3.6	85	36	35
385	300	3.2~3.6	75	18	24
395	300	3.2~3.6	54	14	22
405	300	3.2~3.6	48	11	17

faster under pattern A of LED lamps. The discrepancy in degradation rates of different contaminants was related to the nature of the contaminants themselves. It can be seen that the degradation rate of AR 26 was much faster than that of ACT and DCF. The degradation of AR 26 was not affected by the LED lamp arrangement, that was the different light uniformity. It indicated that the rate-determining step of the degradation of AR 26 was independent of light uniformity. In contrast, the degradation of ACT and DCF was more difficult, and the rate-controlling step was more affected by light uniformity. The results showed that a higher light uniformity was favored.

3.2 Effect of UV-LED Wavelength

Four wavelengths of Tongjia LED lights (365 nm, 385 nm, 395 nm and 405 nm) were selected to investigate the effect of wavelength on the photocatalytic efficiency. As the reaction progressed, the changes in concentrations of AR 26, ACT and DCF were recorded, as shown in Figure 7. The results showed that shorter wavelength UV-LED was more effective for the degradation of AR 26, ACT and DCF. After 360 minutes of reaction, the conversions of AR 26, ACT and DCF were shown in Table 2. At a wavelength of 365nm, the conversion rates of ACT and DCF were significantly improved. This might be related to the activation energy of the degradation reactions of ACT and DCF. Note that the wavelength (λ) is inversely proportional to the photon energy (E). The correlation of $1/\lambda$ and the degradation conversion rate after 360 min is shown in Figure 8. It presented that the degradation rates of the three contaminants were basically linearly related to the photon energy. 365 nm or lower number of wavelengths was better employed for improving the photocatalytic efficiency.

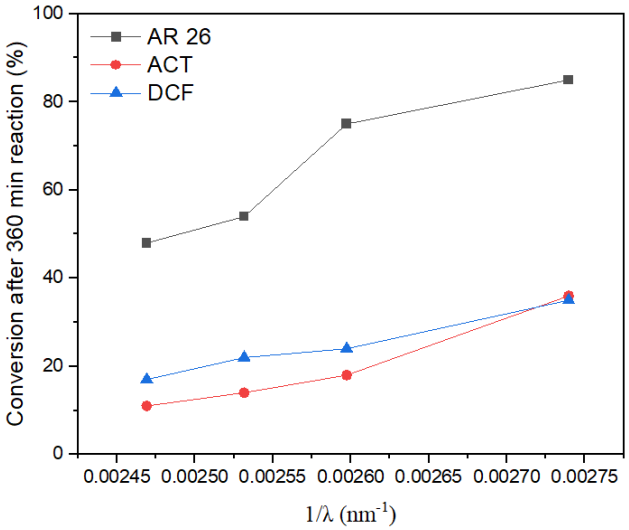

Figure 8. Correlation of degradation efficiency and photon energy (presented as $1/\lambda$) under different wavelengths.

Figure 7(b), 7(d), and 7(f) displayed the degradation rate of AR 26, ACT and DCF. The overall degradation rate under different wavelengths gradually decays. Interestingly, the degradation rate increased slightly at 250 min for AR 26 under four wavelengths. The recovery of the degradation rate indicated that the degradation mechanism had changed at this stage. The photocatalytic degradation of AR 26 compromises oxidation, dealkylation, and cleavage of the methoxy group [28]. Each reaction step will produce different intermediates, such as benzene analogs and anthracene analogs. The degradation rate recovery observed in Figure 7(b) required further research due to the complex reaction network. In contrast, no similar changes in degradation rate were observed for ACT and DCF. This was related to their photocatalytic reaction mechanism, normally involving hydroxylation and decarboxylation. The degradation rate of such two pharmaceutical contaminants was very high at the beginning of the reaction, however, the reaction rate decreased fast and the reaction tended to equilibrium.

3.3 Effect of the Voltage

When solar energy is used as a power source to drive UV-LEDs, the intensity of sunlight will alter the driving voltage of the UV-LEDs, which further decides the output power. Three working voltages (3.0 V, 3.5 V and 4.0 V) were investigated. The theoretical output power and wavelength are listed in Table 3. The concentrations of AR 26, ACT and DCF were recorded (Figure 9). The results showed that work voltage significantly

Table 3. Specification of UV-LED photoreactor with different working voltages and the conversion of AR 26 after 360 min reaction.

Voltage (V)	Output power (mW)	Wavelength (nm)	AR 26 conversion (%)	ACT conversion (%)	DCF conversion (%)
3.0	220	365	69	26	31
3.5	300	365	85	36	36
4.0	408	365	88	40	41

affects the degradation of AR 26, compared with ACT and DCF. A higher working voltage facilitated the photocatalytic degradation of AR 26. This was rationalized that a higher working voltage offered a higher output power. In the early stage of the photocatalytic reaction, the instability of the reaction rate similarly occurred. When the reaction was carried out for 250 minutes, the reaction rate also rebounded. This showed that photocatalytic degradation reactions of AR 26 followed similar reaction kinetics under different light source wavelengths or working voltages. In contrast, the degradation degree and degradation rate of ACT and DCF were not sensitive to the working voltage. The degradation rate was high in the early stage of the reaction but decreased rapidly. After 360 minutes of reaction, the conversions of AR 26, ACT and DCF under

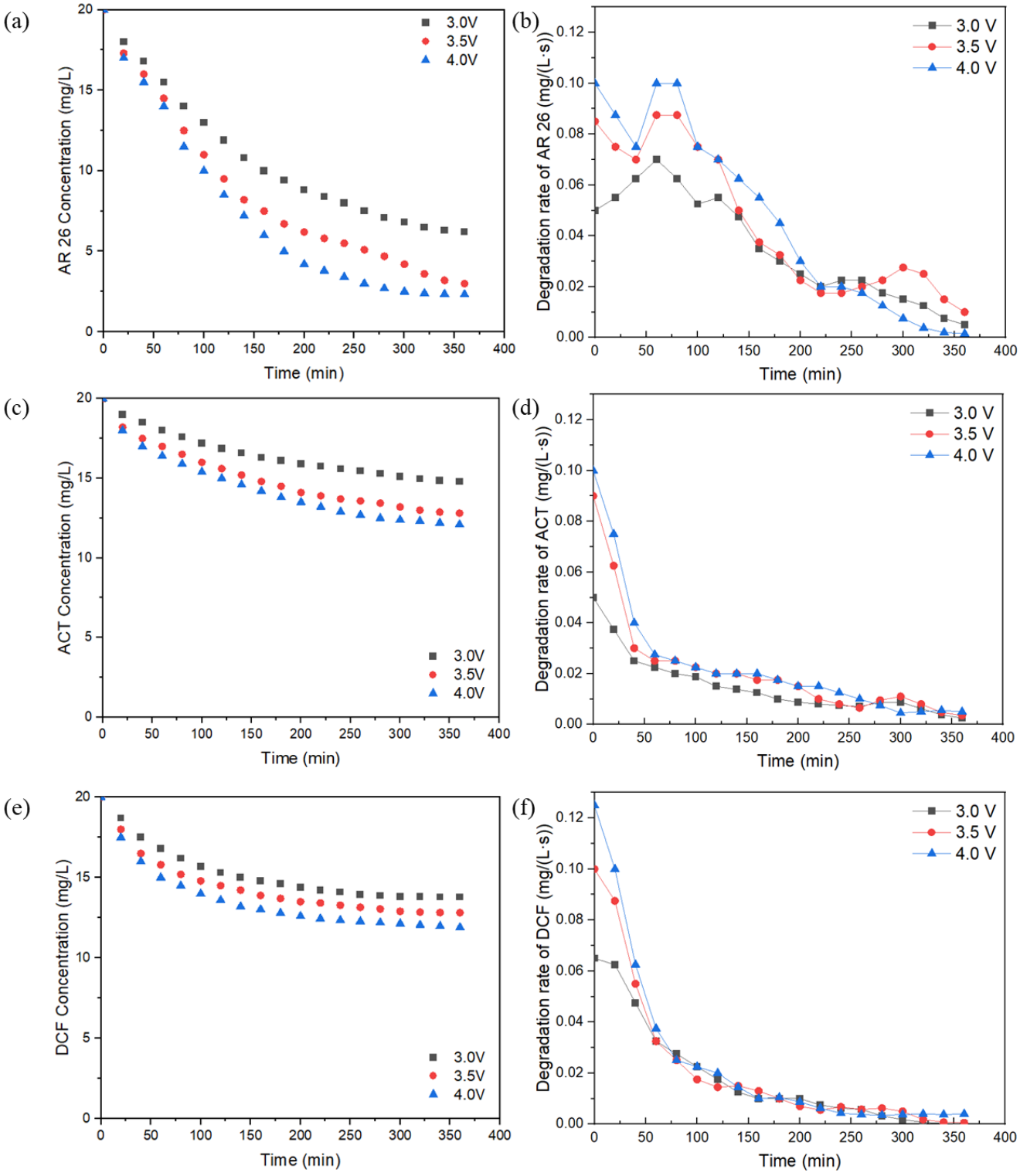

Figure 9. Evolution of the AR 26 concentration and the reaction rate under the different voltages.

different working voltages are shown in Table 3. The correlation of output power with degradation conversion after 360 min was presented in Figure 10. Similar to the results at different wavelengths, the LED output power has a linear relationship with the degradation efficiency. The 4.0 V or a higher working voltage was better employed for improving photocatalytic efficiency.

4. Conclusions

In this work, a homemade photocatalytic test device was set up. The effects of the distribution, wavelength and working voltage of UV LED lamps on the photocatalytic degradation of Acid Red 26, acetaminophen and diclofenac based on TiO_2 catalyst were analyzed. Within the investigated range, higher electrocatalytic efficiency can be achieved on the condition that at 365 nm of LED wavelength, 4.0 V of voltage and 66.5 % of light uniformity. It was found that the output power of the LED light source was a key factor affecting the degradation efficiency of the contaminants. The distribution of LED lights had little impact on the degradation efficiency of AR 26, but had a significant impact on the degradation efficiency of ACT and DCF. This discrepancy was caused by the different rate-determining steps in the degradation reactions for AR 26, ACF and DCF. Wavelengths and working voltages directly determined the output power of LED lamps. Low wavelength and high working voltage improved the photocatalytic degradation rate of AR 26, ACF and DCF. However, different contaminants had different sensitivities to the output power of the LED. This work not only continued the previous optimization of conditions for the AR 26 photocatalytic degradation system, but also used the degradation of two typical pharmaceutical contaminants to verify the system. It helps guide the operating parameters of the TiO_2-based photocatalytic system of UV-LED system application.

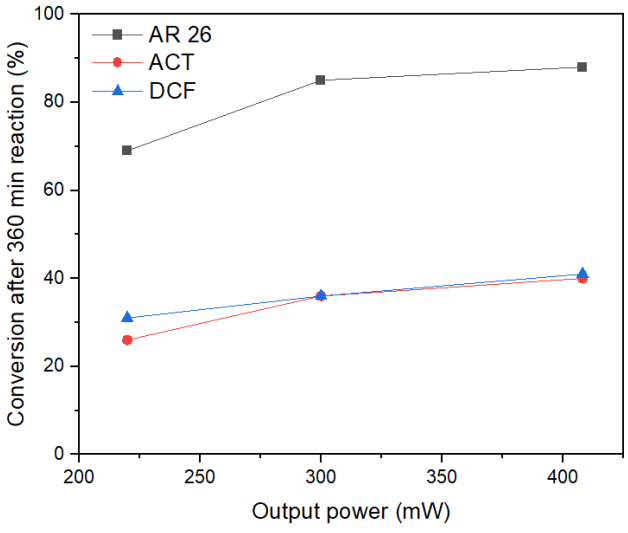

Figure 10. Correlation of degradation efficiency and output power under different working voltages.

CRediT Authors Statement

Zexiang Chen: Conceptualization, Methodology, Investigation, Formal Analysis, Writting Draft Preparation; Chen Wang: Conceptualization, Data Curation, Writing, Visualization, Software; Xue Kang: Validation, Writing, Review and Editing, Data Curation; Yongguo Li: Resources, Review and Editing, Validation, Project Administration. All authors have read and agreed to the published version of the manuscript.

Acknowledgment

Thanks to China National Nuclear Corporation for its support of the centralized R&D project.

References

[1] Dihom, H.R., Al-Shaibani, M.M., Mohamed, R.M.S.R., Al-Gheethi, A.A., Sharma, A., Khamidun, M.H.B. (2022). Photocatalytic degradation of disperse azo dyes in textile wastewater using green zinc oxide nanoparticles synthesized in plant extract: A critical review. *Journal of Water Process Engineering,* 47, 102705. DOI: 10.1016/j.jwpe.2022.1027050

[2] Agarwal, H., Goyal, D. (2022). Photocatalytic degradation of textile dyes using phycosynthesised ZnO nanoparticles. *Inorganic Chemistry Communications,* 142, 109676. DOI: 10.1016/j.inoche.2022.109676

[3] Thanh, N.T.P., Danh, N.T., Nguyen, T.Q., Giang, H.V., Chi, T.K., Giang, L.T.T., Trung, T.Q. (2024). Investigating for Photocatalytic Activity of Hybrid TiO_2/Reduced Graphene Oxide and Application in Reducing VOCs. *Bulletin of Chemical Reaction Engineering & Catalysis*, 19(1), 79-85. DOI: 10.9767/bcrec.20042

[4] Dos Santos, A.B., Cervantes, F.J., Van Lier, J.B. (2007). Review paper on current technologies for decolourisation of textile wastewaters: perspectives for anaerobic biotechnology. *Bioresource Technology,* 98(12), 2369-2385. DOI: 10.1016/j.biortech.2006.11.013

[5] Srinivasan, S., Sadasivam, S.K. (2018). Exploring docking and aerobic-microaerophilic biodegradation of textile azo dye by bacterial systems. *Journal of Water Process Engineering,* 22, 180-191. DOI: 10.1016/j.jwpe.2018.02.004

[6] Ratnawati, R., Enjarlis, E., Husnil, Y.A., Christwardana, M., Slamet, S. (2020). Degradation of Phenol in Pharmaceutical Wastewater using TiO_2/Pumice and O_3/Active Carbon. *Bulletin of Chemical Reaction Engineering & Catalysis,* 15(1), 146-154. DOI: 10.9767/bcrec.15.1.4432.146-154

[7] Bu, J., Yuan, L., Zhang, N., Liu, D., Meng, Y., Peng, X. (2020). High-efficiency adsorption of methylene blue dye from wastewater by a thiosemicarbazide functionalized graphene oxide composite. *Diamond and Related Materials,* 101, 107604. DOI: 10.1016/j.diamond.2019.107604

[8] Thabede, P.M., Shooto, N.D., Naidoo, E.B. (2020). Removal of methylene blue dye and lead ions from aqueous solution using activated carbon from black cumin seeds. *South African Journal of Chemical Engineering,* 33(1), 39-50. DOI: 10.1016/j.sajce.2020.04.002

[9] Bayramoğlu, G., Arıca, M.Y. (2007). Biosorption of benzidine based textile dyes "Direct Blue 1 and Direct Red 128" using native and heat-treated biomass of Trametes versicolor. *Journal of Hazardous Materials,* 143(1-2), 135-143. DOI: 10.1016/j.jhazmat.2006.09.002

[10] Imran, M., Arshad, M., Negm, F., Khalid, A., Shaharoona, B., Hussain, S., Nadeem, S.M., Crowley, D.E. (2016). Yeast extract promotes decolorization of azo dyes by stimulating azoreductase activity in Shewanella sp. strain IFN4. *Ecotoxicology and Environmental Safety,* 124, 42-49. DOI: 10.1016/j.ecoenv.2015.09.041

[11] Ghanbari, F., Moradi, M. (2015). A comparative study of electrocoagulation, electrochemical Fenton, electro-Fenton and peroxi-coagulation for decolorization of real textile wastewater: electrical energy consumption and biodegradability improvement. *Journal of Environmental Chemical Engineering,* 3(1), 499-506. DOI: 10.1016/j.jece.2014.12.018

[12] Balouchi, H., Baziar, M., Dehghan, A., Alidadi, H., Shams, M. (2022). Combination of electrocoagulation and MOF adsorption systems for EBT removal from water. *International Journal of Environmental Analytical Chemistry,* 102(6), 1307-1317. DOI: 10.1080/03067319.2020.1737035

[13] Chiu, Y.-H., Chang, T.-F. M., Chen, C.-Y., Sone, M., Hsu, Y.-J. (2019). Mechanistic insights into photodegradation of organic dyes using heterostructure photocatalysts. *Catalysts,* 9(5), 430. DOI: 10.3390/catal9050430

[14] Chandrabose, G., Dey, A., Gaur, S.S., Pitchaimuthu, S., Jagadeesan, H., Braithwaite, N.S.J., Selvaraj, V., Kumar, V., Krishnamurthy, S. (2021). Removal and degradation of mixed dye pollutants by integrated adsorption-photocatalysis technique using 2-D MoS_2/TiO_2 nanocomposite. *Chemosphere,* 279, 130467. DOI: 10.1016/j.chemosphere.2021.130467

[15] Wang, Y., He, J., Wu, P., Luo, D., Yan, R., Zhang, H., Jiang, W. (2020). Simultaneous Removal of Tetracycline and Cu(II) in Hybrid Wastewater through Formic-Acid-Assisted TiO_2 Photocatalysis. *Industrial & Engineering Chemistry Research,* 59(33), 15098-15108. DOI: 10.1021/acs.iecr.0c02443

[16] Rashed, M.N., El Taher, M.E.D., Fadlalla, S.M. (2022). Photocatalytic degradation of Rhodamine-B dye using composite prepared from drinking water treatment sludge and nano TiO2. *Environmental Quality Management,* 31(3), 175-185. DOI: 10.1002/tqem.21772

[17] Riaz, S., Park, S.-J. (2020). An overview of TiO2-based photocatalytic membrane reactors for water and wastewater treatments. *Journal of Industrial and Engineering Chemistry,* 84, 23-41. DOI: 10.1016/j.jiec.2019.12.021

[18] Song, K., Mohseni, M., Taghipour, F. (2016). Application of ultraviolet light-emitting diodes (UV-LEDs) for water disinfection: A review. *Water Research,* 94, 341-349. DOI: 10.1016/j.watres.2016.03.003

[19] Yung, K.C., Liem, H., Choy, H., Cai, Z. (2014). Thermal investigation of a high brightness LED array package assembly for various placement algorithms. *Applied Thermal Engineering,* 63(1), 105-118. DOI: 10.1016/j.applthermaleng.2013.11.009

[20] Chen, Y., Hou, T., Pan, M. (2019). Comparative analysis between water-cooled and air-cooled heat dissipation in a high-power light-emitting diode chipset. *Journal of Thermal Science and Engineering Applications,* 11(6), 061002. DOI: 10.1115/1.4043004

[21] Seo, J.-H., Lee, M.-Y. (2018). Illuminance and heat transfer characteristics of high power LED cooling system with heat sink filled with ferrofluid. *Applied Thermal Engineering,* 143, 438-449. DOI: 10.1016/j.applthermaleng.2018.07.079

[22] Wang, C., Bai, H., Yi, N., Kang, X. (2023). Multi-dimensional optimization for a novel photocatalytic reactor incorporating the decolorization of azo dye and thermal management of ultraviolet light-emitting diode arrays. *Energy Conversion and Management: X,* 17, 100344. DOI: 10.1016/j.ecmx.2022.100344

[23] Giri, A.S., Golder, A.K. (2014). Fenton, Photo-Fenton, H2O2 Photolysis, and TiO2 Photocatalysis for Dipyrone Oxidation: Drug Removal, Mineralization, Biodegradability, and Degradation Mechanism. *Industrial & Engineering Chemistry Research,* 53(4), 1351-1358. DOI: 10.1021/ie402279q

[24] Eskandarian, M.R., Choi, H., Fazli, M., Rasoulifard, M.H. (2016). Effect of UV-LED wavelengths on direct photolytic and TiO_2 photocatalytic degradation of emerging contaminants in water. *Chemical Engineering Journal,* 300, 414-422. DOI: 10.1016/j.cej.2016.05.049

[25] Moghni, N., Boutoumi, H., Khalaf, H., Makaoui, N., Colón, G. (2022). Enhanced photocatalytic activity of TiO_2/WO_3 nanocomposite from sonochemical-microwave assisted synthesis for the photodegradation of ciprofloxacin and oxytetracycline antibiotics under UV and sunlight. *Journal of Photochemistry and Photobiology A: Chemistry,* 428, 113848. DOI: 10.1016/j.jphotochem.2022.113848

[26] Wang, J., Lee, S.R., Zou, H. (2016). *Effect of the surface curvature of the phosphor layer on the optical performance of a WLED.* Paper presented at the 2016 13th China International Forum on Solid State Lighting (SSLChina).

[27] Institute, A.N.S. (1997). Electronic projction-fixed resolution projectors. In. New York: National Association of Photographic Manufacturers, Inc.

[28] Al-Zahrani, S. A., Patil, M. B., Mathad, S. N., Patil, A. Y., Al Otaibi, A., Masood, N., Mansour, D., Kha, A., Gupta, V., Topare, N.S., Somya, A., Ayyar, M. (2023). Photocatalytic Azo Dye Degradation Using Graphite Carbon Nitride Photocatalyst and UV-A Irradiation. *Crystals,* 13(4), 577. DOI: 10.3390/cryst13040577